CCSP Deliverable D416
Espoo 2016

Kimmo Korhonen
Lasse Ahonen
Nicklas Nordbäck

Geothermal and geochemical constraints of liquid CO_2 storage in rock caverns

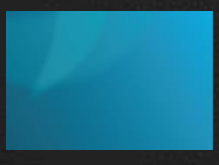

ccsp
Carbon Capture and Storage Program

CLIC Innovation Oy
ETELÄRANTA 10
P.O. BOX 10
FI-00131 HELSINKI
FINLAND
www.clicinnovation.fi

CLIC Innovation Oy
Carbon Capture and Storage Program (CCSP)
Deliverable D416

Kimmo Korhonen
Lasse Ahonen
Nicklas Nordbäck

Geothermal and geochemical constraints of liquid CO_2 storage in rock caverns

Report Title: Geothermal and geochemical constraints of liquid CO_2 storage in rock caverns

Key words: carbon dioxide, intermediate storage, rock caverns, geochemistry, geothermal modelling

Abstract

Carbon capture and storage (CCS) may require the transport of CO_2 over long distances in order to reach the final CO_2 storage site which warrants intermediate storage of the captured CO_2. Here we present an investigation of some of the geothermal and geochemical aspects of the intermediate storage of CO_2 in its liquid form in underground rock caverns and present a general emplacement strategy for such stores based on the results of numerical simulations.

Favourable temperature-pressure conditions for storing liquid CO_2 are below-zero centigrade temperatures and above 10-bar pressures. The storage of cold liquid CO_2 in a rock cavern will cool the ambient bedrock and create an expanding frozen zone around the store. This frozen zone is an essential aspect of intermediate storage as it helps to seal the CO_2 inside the store.

Numerical simulations of the geothermal evolution of intermediate CO_2 storage in rock caverns were carried out in order to investigate the energy demand and the growth of the frozen zone. Storing cold liquid CO_2 in warm bedrock will induce a large heat flow into the store that boils off the liquid CO_2. The boil-off needs to be re-liquefied requiring energy which is relative to the magnitude of the heat flow. Simulations without a pre-cooling period indicate that approximately a one-megawatt cooling capacity would needed during the first years of storage in order to keep the CO_2 liquid after which the cooling demand drops below 200 kW. Pre-cooling the ambient bedrock using a constant cooling power closer to the long-term cooling demand would, thus, be warranted in order to keep the cooling capacity requirement reasonable.

Several store designs and depths were considered. The simulations indicate that the CO_2 storage temperature has a more significant influence on the energy demand than the store depth. However, simulations of shallow stores indicate that the heat flux through the ground surface will inhibit the growth of the frozen zone. Thus, stores should be located deep enough. Furthermore, the prevailing hydrostatic pressure, in the case of shallow stores, is low which would also require low CO_2 storage temperatures in order to make the CO_2 vapour pressure low enough. This, consequently, leads to larger energy demands.

The simulations indicate that the most favourable store depth is 100 metres or deeper and the most favourable storage temperature is between −20 and −40 °C. In these cases the prevailing hydrostatic pressure best matches the CO_2 vapour pressure and the thickness of the frozen zone is likely to grow thick enough to ensure safe containment of CO_2 inside the store.

Espoo 2016

Table of contents

1 Introduction

Large amounts of carbon dioxide (CO_2) are generated by fossil fuel power plants and in industrial processes. Modern technology allows the capture of most of this waste CO_2 at its sources before it enters the Earth's atmosphere and raises the atmospheric CO_2 concentration. The captured CO_2 can be geologically stored outside the Earth's carbon cycle in order to prevent further increases of the atmospheric CO_2 concentration. This technology is called carbon capture and storage (CCS).

Because the CO_2 sources are typically located far away from the final storage locations, CO_2 needs to be transported long distances. Such transport often requires the intermediate storage of CO_2 before its shipping to the final storage site. This is, for example, the case for Finland where there are no suitable geological formations for the final storage of CO_2. Intermediate storage is typically realized using steel tanks located above the ground surface. However, when the volume of CO_2 that needs to be stored grows above 50,000 m^3, storage in rock caverns becomes a more attracting solution (Ritola et al., 2014).

The final storage (or sequestration) of CO_2 in geological formations has received much attention in the literature (e.g., Leung et al., 2014; Myer, 2011; Fang et al., 2010). Such formations comprise deep saline aquifers, and depleted oil and gas reservoirs. However, intermediate storage of CO_2 in caverns excavated in hard crystalline bedrock is a new approach to intermediate storage that has yet to be tested (Ritola et al., 2014).

Here we investigate the chemical and thermal aspects of the intermediate storage of CO_2 in rock caverns excavated in hard crystalline bedrock and envisage a general emplacement strategy for the storage. The intermediate storage of CO_2 is considered to be carried out in its liquid form. This is mainly because of the following two factors. Firstly, CO_2 is already transported in its liquid form. Secondly, CO_2 is denser in this form than in its gaseous form which allows larger volumes to be stored. However, in its liquid form, CO_2 needs to be stored in a high pressure and low temperature. This presents limiting conditions to the storage of CO_2 in a rock cavern.

2 Storage principle

The fundamental premise for the intermediate storage of CO_2 in an underground rock cavern is that it is carried out in its liquid form. Carbon dioxide occurs as a liquid in high pressures and low temperatures (see Fig. 1). The most favourable conditions occur near the saturation line and close to the triple point where the pressure and temperature are at their lowest while CO_2 remains a liquid.

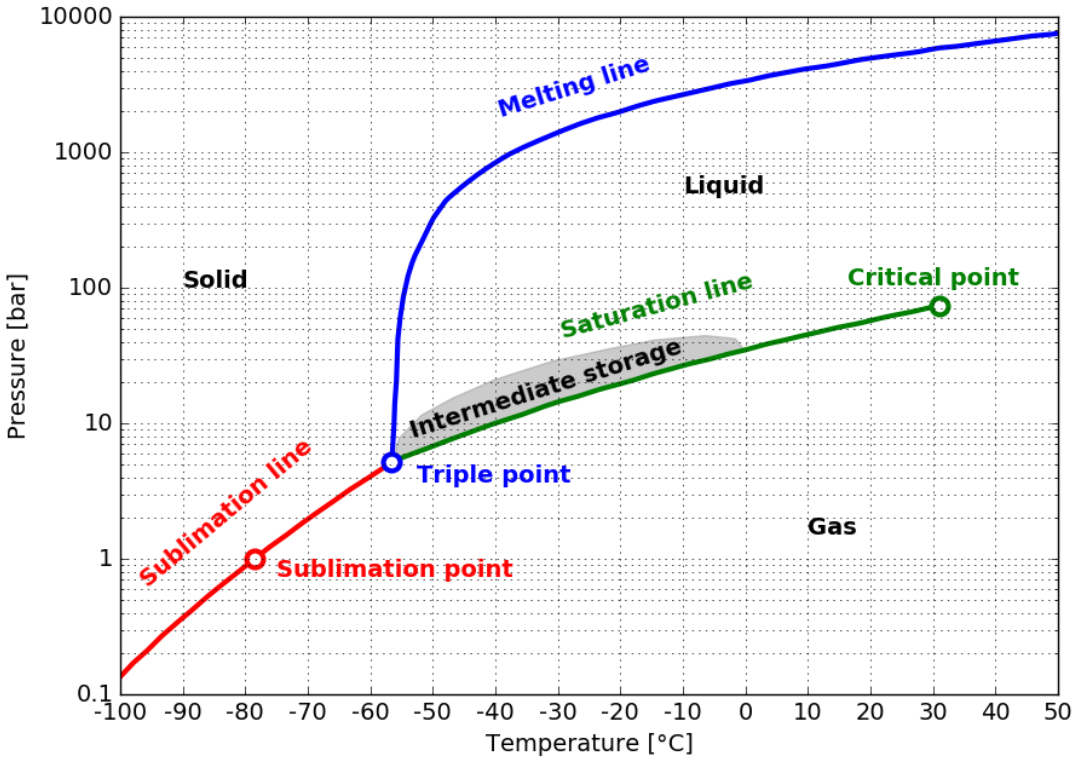

Figure 1. *Carbon dioxide phase diagram. The grey area indicates the favourable temperature-pressure conditions for intermediate storage of CO_2 in a rock cavern.*

The temperature difference between the cold liquid CO_2 and the warm ambient bedrock creates a heat flow into the store which boils off the liquid CO_2. The boil-off gas (BOG) needs to be re-liquefied which requires energy. The demand for energy depends on the temperature of the ambient bedrock which rises as a function of depth. Moreover, the BOG may escape from the storage through fractures and enter the atmosphere. Therefore, the cavern should be located well below the groundwater level so that fractures are saturated with groundwater. In addition, the hydrostatic pressure should exceed the CO_2 gas pressure sealing the CO_2 into the cavern. However, the cooling of the ambient bedrock by cold liquid CO_2 creates an expanding zone within which fracture water is frozen. This zone presents a barrier which is likely to be impermeable to pressure and may allow the storage of CO_2 at shallower depths.

3 Liquid CO_2 and its interactions

The storage of liquid natural gas (LNG) and liquid petroleum gas (LPG) in hard rock caverns carry similarities to the intermediate storage of CO_2 (Ritola et al., 2014). In contrast to LPG and LNG, CO_2 molecules dissolve fairly well in water. However, the dissolution and diffusion of CO_2 in ice are negligible. That is, a frozen zone is needed around the intermediate CO_2 store also to prevent the CO_2 from dissolving in water. Diffusion studies of CO_2 in gas bubbles in Antarctic ice cores have shown excellent

preservation of the original gas phase at time scales of hundreds of thousands years (Ahn et al., 2008).

Interaction between liquid CO_2 and a rock wall might be a potential source of impurities in the liquid phase. The pure liquid form of CO_2 can be considered as an inert phase towards the solid rock surface. However, the phase boundary may also include micro-environments where ice and the CO_2 vapor phase interact as boil-off occurs. In principle, CO_2 and water together form carbonic acid, which may dissolve carbonate minerals in rocks. For example, Bateman et al. (2013) reported a 5-year experimental study on the interactions between supercritical CO_2 (at 80 bars and 30 °C) and clay-rich, slightly carbonaceous (2.4% calcite) Utsira caprock from the Sleipner gas field. Their results indicate the release of Ca molecules from calcite dissolution, but no other clear mineralogical changes, even though the liquid phase of water was present. That is, host rocks that are rich in carbonate minerals are not favourable for the intermediate storage of CO_2.

4 Finite element simulations

4.1 Conceptual model

Intermediate CO_2 storage was conceptualized in the following way. The store is located in Southern Finland and is a cavern that is excavated in hard granitic or gneissic bedrock which is low in calcite. There is no groundwater movement so that heat transfer occurs purely conductively. The store capacity is 50,000 m^3. The bedrock is either intact, or slightly porous (0.5% porosity) in which case the pore spaces are saturated with groundwater. The bedrock contains radioactive elements that produce heat. Heat is also conducted from greater depths by the geothermal gradient. The ground surface is exposed to solar and atmospheric radiation. The surface is also exposed to the atmosphere including wind and rain. The ground surface radiates heat according to its temperature as a black body.

Carbon dioxide is stored in a cavern which is located at a specific depth at which a specific hydrostatic pressure prevails (Table 1). The storage is carried out in the liquid form of CO_2 at a specific temperature and pressure (Table 2).

Table 1. *Store depths at which CO_2 is considered to be stored in a hard rock cavern and the prevailing hydrostatic pressures at those depths. The height of the water column is assumed to be equal to the store depth.*

Store depth [m]	Hydrostatic pressure [bar]
50	4.9
100	9.8
150	14.7
200	19.6

250	24.5
300	29.3

Table 2. *Temperatures and pressures at which CO_2 is liquid and is considered to be stored in a hard rock cavern.*

Storage temperature [°C]	Carbon dioxide gas pressure [bar]
−5	30.5
−10	26.5
−20	19.5
−30	14.2
−40	10.0

4.2 Simulation scenarios

Intermediate storage of CO_2 in a hard rock cavern was simulated by solving a finite element model which implemented the above conceptual model in time. Because depositing cold liquid CO_2 directly to the store surrounded by warm ambient bedrock would create a large temperature disturbance which would result in a large heat flow into the store, two storage scenarios were considered. In the first scenario, CO_2 was simply deposited to the store while ignoring the adverse effects of a large heat flow. In the second scenario, the bedrock in the vicinity of the store was first cooled using a constant cooling power until the average cavern wall temperature reached the CO_2 storage temperature. After the pre-cooling period, CO_2 was deposited into the store.

4.3 Model geometries

Two store designs were considered: the single and dual cavern stores. The single cavern store consists of a single long cavern while the dual cavern store consists of two shorter caverns running in parallel and separated by a distance of 40 meters (Fig. 2).

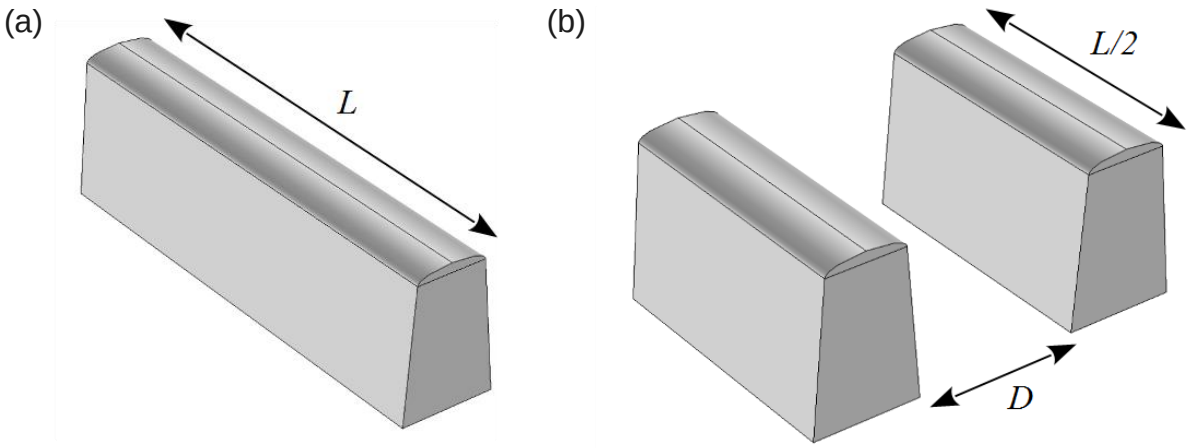

Figure 2. *Store designs. (a) The single and (b) dual cavern stores of length L. The cavern separation D was 40 meters.*

The cavern profile was modeled after crude oil caverns that are known to have excellent stability characteristics (Johansson, 1985). In addition, two cavern profiles of different sizes were used to investigate the influence of the profile size. Fig. 3 shows the cavern profiles tested and their dimensions. The lengths of the stores were calculated such that the store volume was 50,000 m^3. Table 3 enumerates the store designs and the respective cavern lengths.

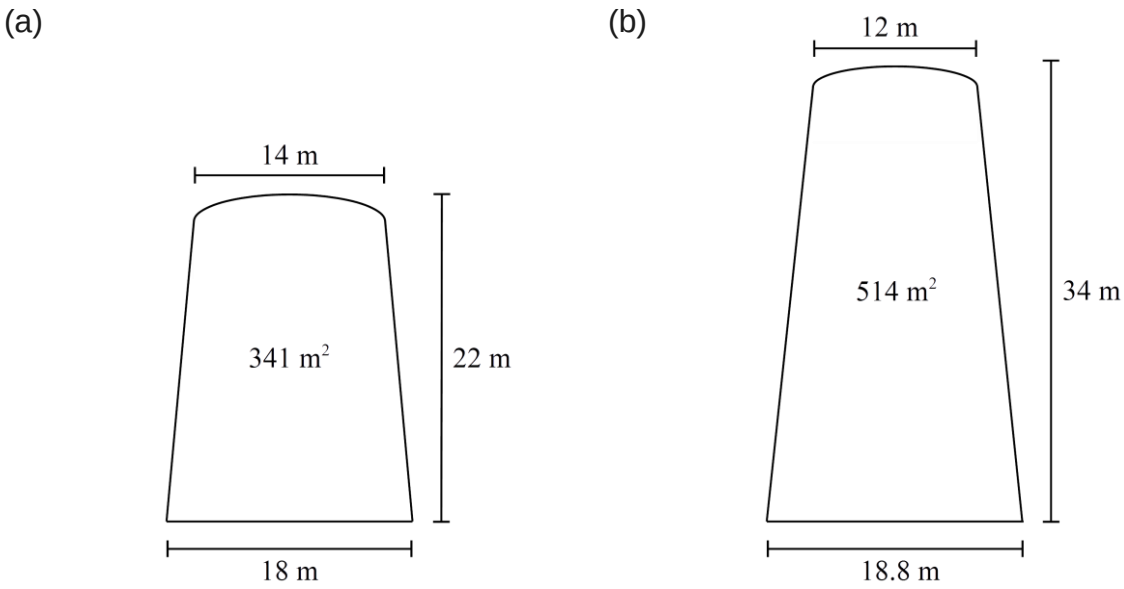

Figure 3. *Cavern profiles and their dimensions. (a) The small and (b) large cavern profiles.*

Table 3. *Store designs and their respective cavern lengths.*

Store design	Cavern length [m]
Single cavern store of small profile size	146
Single cavern store of large profile size	97

Dual cavern store of small profile size	73
Dual cavern store of large profile size	49

Both store designs contained two symmetry planes through which there was no heat flow (Fig. 4a and 4b). Thus, only a quadrant of the complete 3D geometry needed to be modeled (Fig. 4c and 4d). Furthermore, the storage of CO_2 was modeled using boundary conditions imposed on the cavern wall so that the cavern volume was carved out of the model geometry (Fig. 5) and was not modelled.

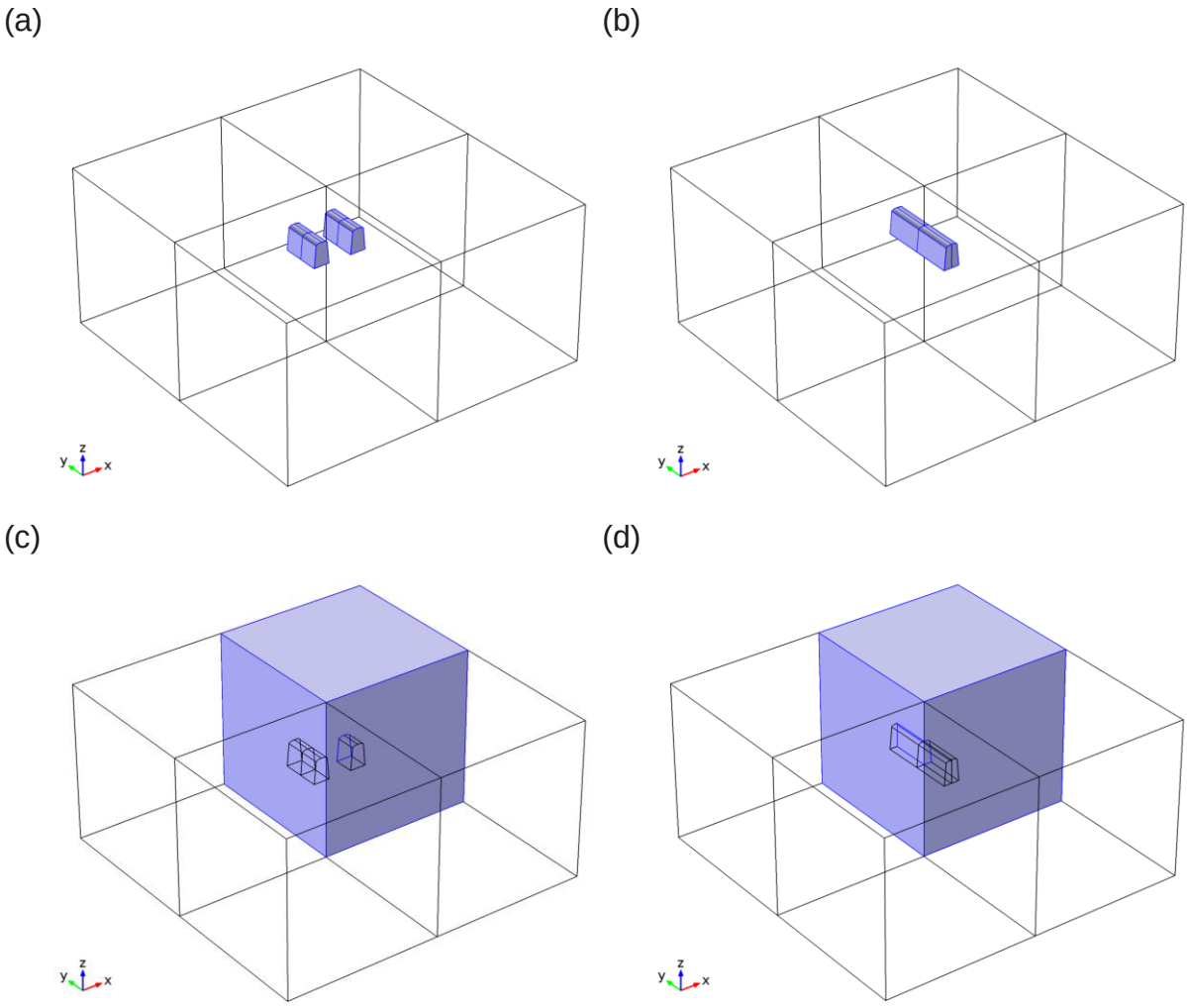

Figure 4. *Schematic illustration of the symmetry planes and modelled quadrants. (a) The single and (b) dual cavern store geometries and their symmetry planes. The modelled quadrant of the (c) single and (b) dual cavern models.*

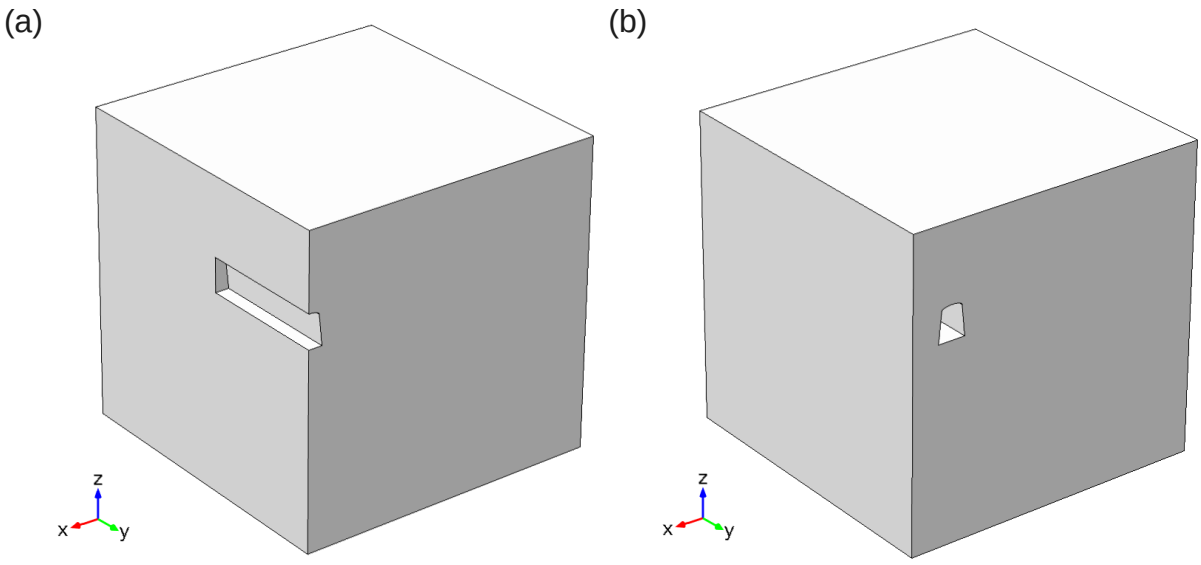

Figure 5. *Schematic illustration of the (a) single and (b) dual cavern store geometries.*

4.4 Governing equation

The partial differential equation describing conductive heat transfer is

$$\rho \cdot C_p \cdot \frac{\partial T}{\partial t} = \nabla \cdot (k \cdot \nabla T) + Q_{\text{radiogenic}}, \quad (1)$$

where ρ is the density of the medium, C_p is the specific heat capacity of the medium at constant pressure, T is the temperature distribution in the medium, t is time, k is the thermal conductivity of the medium and $Q_{\text{radiogenic}}$ is the radiogenic heat production in the medium. When the bedrock was assumed to be porous, the material properties in Eq. (1) were modelled as equivalent properties defined as the volumetric averages

$$\rho = (1-\theta) \cdot \rho_{\text{bedrock}} + \theta \cdot \rho_{\text{groundwater}}, \quad (2)$$

$$k = (1-\theta) \cdot k_{\text{bedrock}} + \theta \cdot k_{\text{groundwater}} \quad (3)$$

and

$$C_p = \frac{(1-\theta) \cdot \rho_{\text{bedrock}} \cdot C_{p,\text{bedrock}} + \theta \cdot \rho_{\text{groundwater}} \cdot C_{p,\text{groundwater}}}{(1-\theta) \cdot \rho_{\text{bedrock}} + \theta \cdot \rho_{\text{groundwater}}}, \quad (4)$$

where θ is the liquid fraction (porosity) of the rock matrix, $1-\theta$ is the solid fraction of the rock matrix, k_{bedrock} and $k_{\text{groundwater}}$ are the thermal conductivities of the bedrock and the pore-filling groundwater respectively, ρ_{bedrock} and $\rho_{\text{groundwater}}$ are the volumetric heat capacities of the bedrock and groundwater respectively, and $C_{p,\text{granite}}$

and $C_{p,groundwater}$. are the specific heat capacities of the bedrock and groundwater at constant pressure respectively.

4.5 Boundary conditions

Four different boundary conditions were applied to the boundaries of the models. Fig. 6 indicates these boundary conditions and the boundaries to which they were applied.

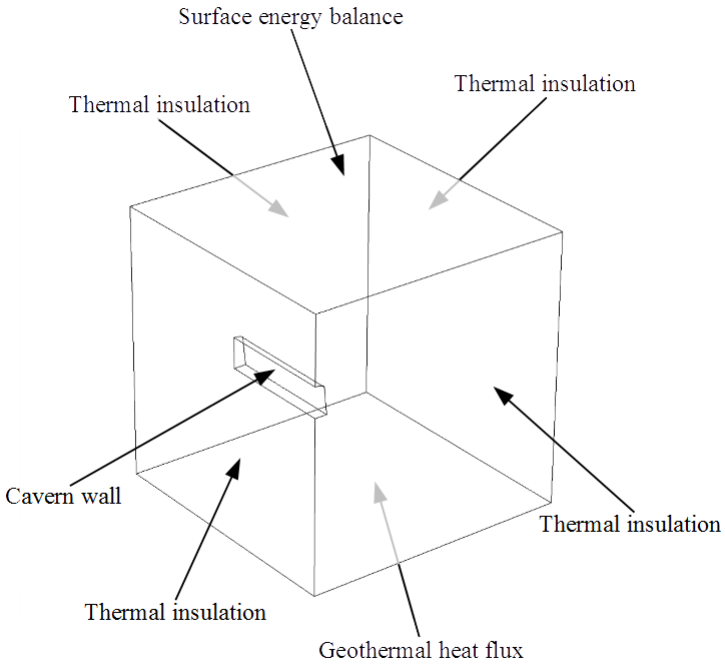

Figure 6. *Schematic illustration of the boundary conditions and the surfaces to which they were applied.*

4.5.1 Top boundary

The top boundary was assigned the outward heat flux boundary condition

$$-k \cdot \frac{\partial T}{\partial z} = G, \tag{5}$$

where G is the conductive heat flux from the ground into the atmosphere which was solved from the ground surface energy balance equation

$$R_{net} = G + H + L_{vapour} \cdot E, \tag{6}$$

where R_{net} is the net radiation incident on the ground surface, H is the turbulent sensible heat flux and $L_{vapour} \cdot E$ is the turbulent latent heat flux (L_{vapour} is the latent heat of vaporization of water, 2245 kJ/kg, and E is evaporation from the ground surface) (e.g., Deardorff, 1978).

The net radiation was given by

$$R_{\text{net}} = (1-\alpha)\cdot Q_{\text{solar}} + \varepsilon_{\text{ground}} \cdot (Q_{\text{atmosphere}} - \sigma \cdot T_{\text{ground}}^4), \quad (7)$$

where α is the albedo of the ground surface, Q_{solar} is the incoming solar radiation, $\varepsilon_{\text{ground}}$ is the emissivity of the ground surface, $Q_{\text{atmosphere}}$ is the thermal radiation emitted by the atmosphere, σ is the Stefan-Boltzmann constant ($5.670373 \cdot 10^{-8}$ W/m^{2}K^4) and T_{ground} is the ground temperature (e.g., Deardorff, 1978). The sensible heat flux was modelled using

$$H = h \cdot (T_{\text{ground}} - T_{\text{air}}), \quad (8)$$

where T_{air} is the air temperature and h is the turbulent convective heat transfer coefficient.

4.5.2 Bottom boundary

The bottom boundary was assigned the inward heat flux boundary condition

$$k \cdot \frac{\partial T}{\partial z} = q_{\text{geo}}, \quad (9)$$

where q_{geo} is the geothermal heat flux into the model domain.

4.5.3 Vertical boundaries

The vertical boundaries were assigned the adiabatic (or no-flux) boundary condition

$$k \cdot \frac{\partial T}{\partial n} = 0, \quad (10)$$

where n is the direction normal to the surface (either the x or y direction).

4.5.4 Cavern wall boundary

In simulations containing only a storage period, the cavern walls were assigned the temperature boundary condition. In these simulations, the cavern wall temperature was gradually decreased from the initial bedrock temperature to the storage temperature during the first simulated month. This was necessary in order to avoid large temperature gradients at the cavern walls that would have caused numerical instabilities.

In simulations containing both an initial cooling period and a storage period, two different boundary conditions were applied on the cavern walls. In the beginning of the cooling period, the cavern walls were assigned the heat flux boundary condition

$$-\mathbf{n} \cdot (-k \cdot \nabla T) = -\frac{Q_{\text{cooling}}}{A_{\text{walls}}}, \quad (11)$$

where **n** is the outward unit normal to the boundary, $Q_{cooling}$ is the cooling capacity and A_{walls} is the surface area of the cavern walls. The heat flux due to the cooling was gradually increased from 0 to its full value during the first month of the cooling period in order to avoid numerical instabilities. The heat flux boundary condition was in effect until the average temperature of the cavern walls reached the storage temperature. Then, the boundary condition was changed to the constant temperature boundary condition which was used to set the cavern wall temperature to the storage temperature for the rest of the simulation.

4.6 Parameter values and functions used in the simulations

4.6.1 Initial ground temperature

The initial ground temperature profile for the simulations was calculated using a 1D model that was equivalent to the 3D models in all aspects disregarding the carbon dioxide store. The 1D model was initialized with an arbitrary temperature distribution and was run until a balance was reached between the geothermal and surface heat fluxes. The resulting temperature distribution for the 1st of January (Fig. 7) was used to initialize the temperatures in the 3D simulations.

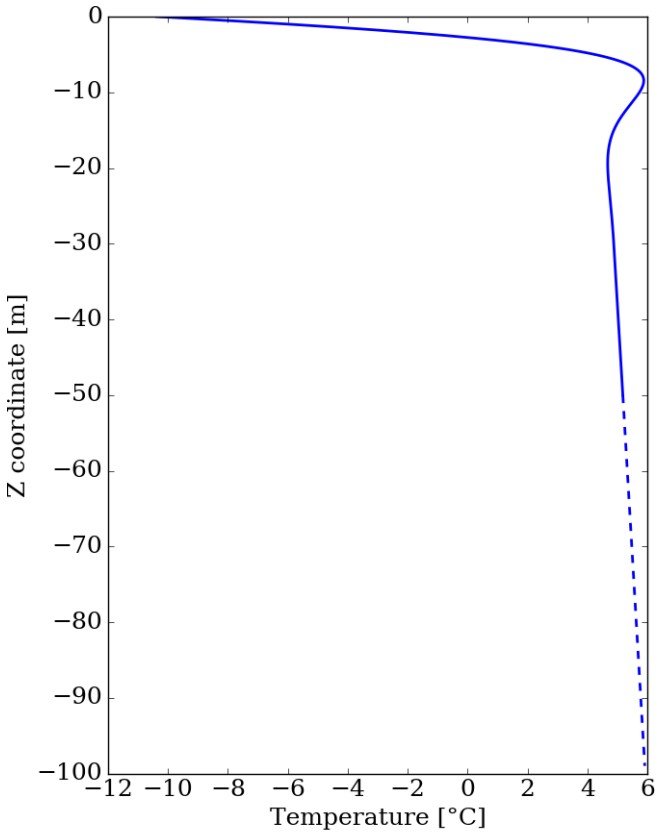

Figure 7. *Initial ground temperature profile for the 3D simulations (1st of January).*

4.6.2 Surface energy balance

Periodical functions were devised for solar radiation, atmospheric radiation, air temperature, albedo and ground emissivity for use in the ground surface boundary condition given in Eqs. (6)–(8). The functions were of the general form

$$f(t) = A \cdot \sin(\omega \cdot t + \varphi) + c\,, \tag{12}$$

where A is the amplitude, ω is the angular frequency of one year ($2 \cdot \pi / 365.2425 \cdot 86400$ 1/s), φ is the phase offset and c is a coefficient. The parameters A, φ and c were estimated by fitting the functions to data using the Levenberg-Marquardt optimization method (e.g., Nocedal and Wright, 2006).

The solar radiation, atmospheric radiation and air temperature functions were based on data obtained for Southern Finland (latitude 60.5 °N and longitude 25.5 °E) from the Surface and Solar Energy (SSE) web portal (supported by the NASA LaRC POWER Project) of the Atmospheric Science Data Center of NASA Langley Research Centre (https://eosweb.larc.nasa.gov/cgi-bin/sse/sse.cgi). Fitting Eq. (12) to the data resulted in the functions

$$Q_{\text{solar}} = 117.408 \cdot \sin(\omega \cdot t + 4.930) + 117.408\,, \tag{13}$$

$$Q_{\text{atmosphere}} = 52.299 \cdot \sin(\omega \cdot t + 4.302) + 284.525 \tag{14}$$

and

$$T_{\text{air}} = 12.243 \cdot \sin(\omega \cdot t + 4.365) + 4.097 \tag{15}$$

(see Fig. 8).

The albedo function was based on data obtained for Jokioinen, Southern Finland from the Global Energy Balance Archive (http://www.geba.ethz.ch) (Gilgen and Ohmura, 1999) of the Swiss Federal Institute of Technology in Zürich. Fitting a modified version of Eq. (12) to the data resulted in the function

$$\text{albedo} = \max(0.125 \cdot \sin(\omega \cdot t + 0.572) + 0.092,\ 0.092) \tag{16}$$

(see Fig. 9). Because the albedo is fairly constant during the summer and early autumn, Eq. (12) was modified to better incorporate this property of the annual albedo variation by not allowing values below 0.092 using the max function.

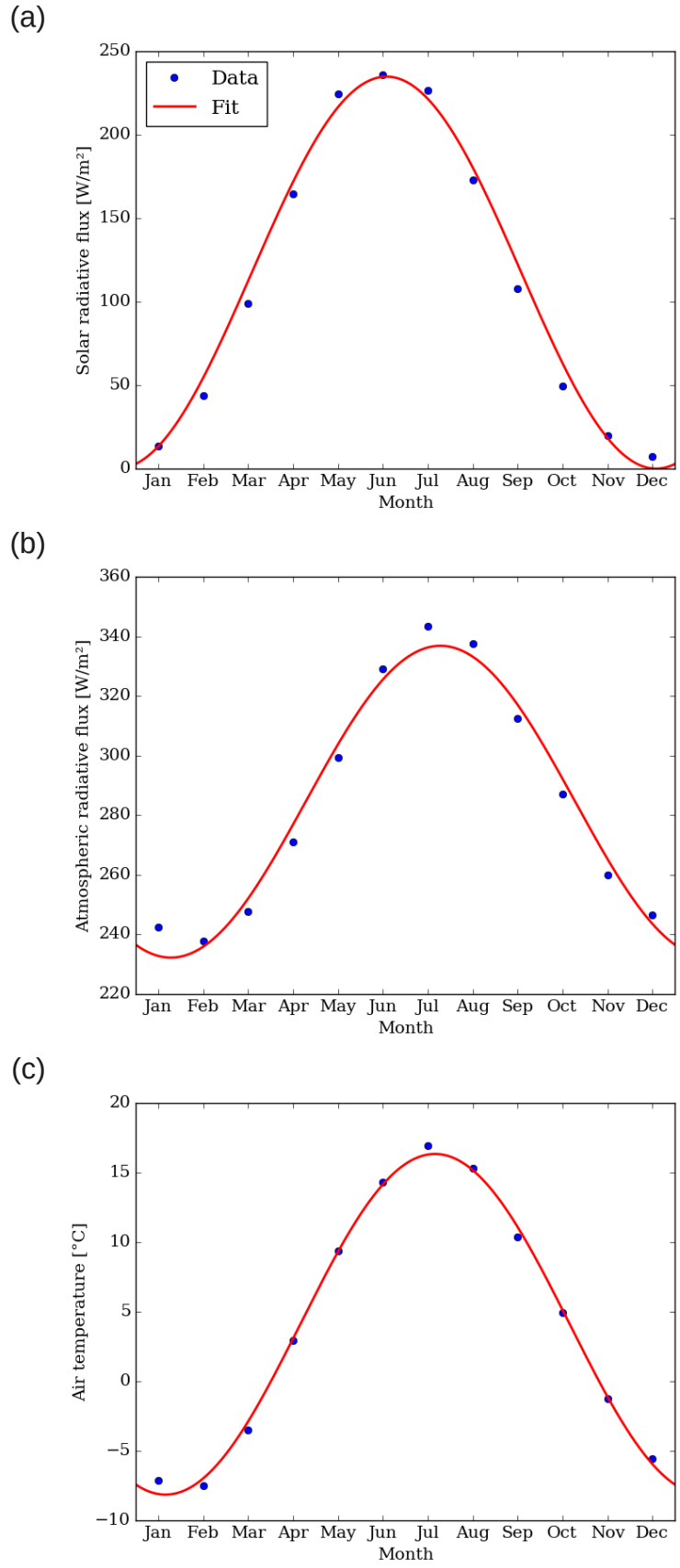

Figure 8. *Solar radiation, atmospheric radiation and air temperature data for Southern Finland and the functions fitted to the data.*

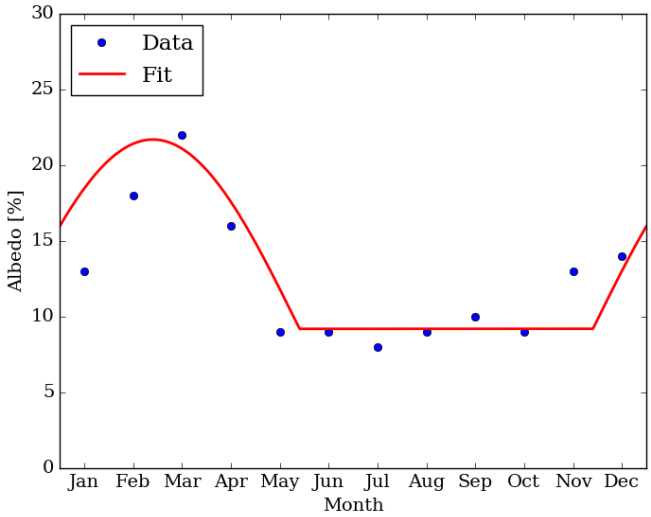

Figure 9. *Albedo data for Jokioinen, Southern Finland, and the function fitted to the data.*

The ground emissivity function was based on data obtained for Southern Finland (latitude 60.5 °N and longitude 25.5 °E) from the University of Wisconsin-Madison Baseline Fit Emissivity Database (http://cimss.ssec.wisc.edu/iremis/) (Seeman et al., 2007). Fitting Eq. (12) to the data resulted in the function

$$\varepsilon_{ground} = 0.009 \cdot \sin(\omega \cdot t + 0.399) + 0.976 \quad (17)$$

(see Fig. 10).

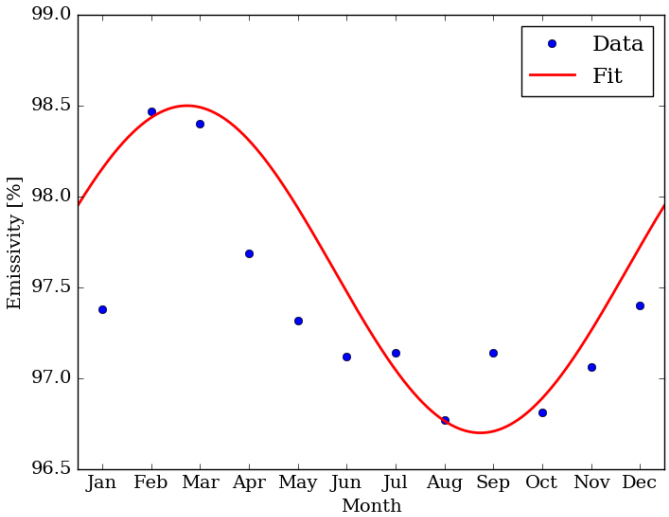

Figure 10. *Ground emissivity data for Southern Finland and the function fitted to the data.*

4.6.3 Parameter values for the simulations

Table 4 lists simulation parameters and the values chosen for them. The dimensions of the solution domain were chosen so that its boundaries were located far enough

from the store so as not to influence the solution. Values for the thermal and other parameters were chosen to reflect the average climatic and geological conditions prevalent in Southern Finland. The cooling power was chosen so that the duration of the cooling period would not exceed three years. The duration of the storage period was chosen to be sufficiently long as to reach a near steady-state heat flow.

Table 4. *Parameters and their values used in the simulations of intermediate storage of CO_2 in a hard rock cavern.*

Parameter (symbol)	Value
Width of solution domain	500 m
Height of solution domain	700 m
Geothermal heat flux (q_{geo})	45 mW/m^2
Radiogenic heat production ($Q_{radiogenic}$)	1.5 μW/m^3
Heat transfer coefficient (h)	20 W/m^{2}K
Thermal conductivity of bedrock (k_{rock})	3 W/mK
Specific heat capacity of bedrock ($C_{p,rock}$)	700 J/kgK
Density of bedrock (ρ_{rock})	2700 kg/m^3
Thermal conductivity of water (k_{water})	0.56 W/mK
Specific heat capacity of water ($C_{p,water}$)	4186 J/kgK
Density of water (ρ_{water})	999 kg/m^3
Thermal conductivity of ice (k_{ice})	2.22 W/mK
Specific heat capacity of ice ($C_{p\ ice}$)	2050 J/kgK
Density of ice (ρ_{ice})	916 kg/m^3
Porosity of bedock (θ)	0.5 %
Average annual precipitation (p_{annual})	600 mm
Average annual evaporation ($E = \rho_{water} \cdot p_{annual}$)	599.4 kg/m^2
Cooling power ($Q_{cooling}$)	200 kW
Duration of the storage period	100 a

4.7 Computational mesh

The computational meshes consisted of a lower and an upper part (Fig. 11a). The lower part extended from the depth of 700 meters to the depth of 30 metres and contained the cavern walls. The cavern walls were meshed first using triangles with the maximum side length of 1 meter (Fig. 11b) in order to solve Eq. (1) with sufficient accuracy in the vicinity of the store. The rest of the lower part was meshed using tetrahedrons with the maximum side length of 38.5 meters. The upper part of the

mesh was constructed by sweeping the triangle mesh that was generated at the top boundary of the lower part (the horizontal boundary at the depth level of 30 meters) to the ground surface at 1 meter intervals in order to solve temporal and spatial changes in the ground temperature with sufficient accuracy. The resulting numbers of elements for each computational mesh are listed in Table 5.

(a)

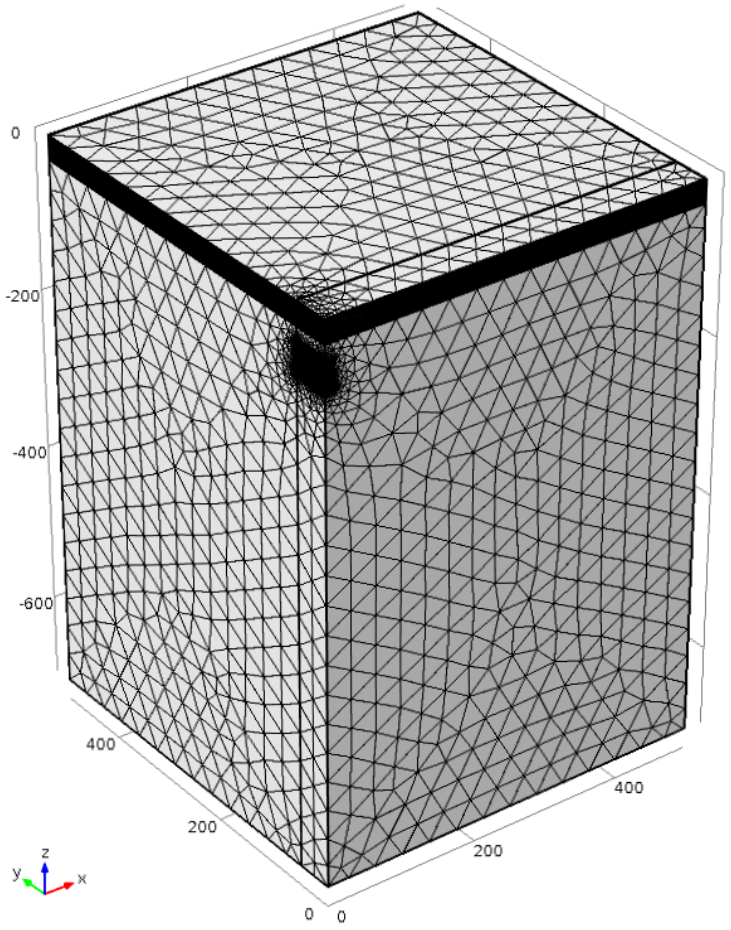

(b)

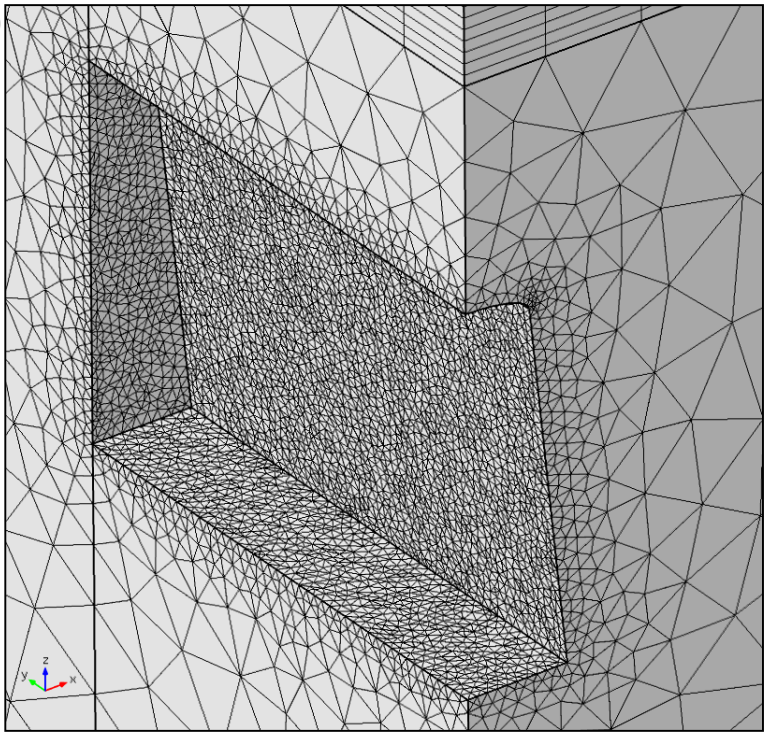

Figure 11. *Example of the computational mesh for the single cavern store model of large profile size. (a) The mesh for the complete model with a lower and upper part, and (b) a close up of the mesh around the cavern.*

Table 5. *Numbers of elements in the computational meshes.*

Store design	Number of elements
Single cavern of small cavern profile size	132,978
Single cavern of large cavern profile size	129,667
Dual cavern of small cavern profile size	144,118
Dual cavern of large cavern profile size	139,191

5 Results

Seven series of simulations were run (Table 6). Each series of simulations consisted of simulation runs for all combinations of the store depths of −50, −100, −150, −200, −250 and −300 meters (Table 1) and the storage temperatures of −5, −10, −20, −30 and −40 °C (Table 2). That is, each series of simulations consisted of 30 individual runs.

Table 6. *Carbon dioxide store simulations ran.*

Simulation series	Store design	Pre-cooling	Porosity [%]
#1	Single cavern of small cavern profile	No	0.0
#2	Dual cavern of small cavern profile	No	0.0
#3	Single cavern of small cavern profile	Yes	0.0
#4	Dual cavern of small cavern profile	Yes	0.0
#5	Single cavern of large cavern profile	Yes	0.0
#6	Dual cavern of large cavern profile	Yes	0.0
#7	Single cavern of large cavern profile	Yes	0.5

5.1 Heat flow and heat flux into the store

Figures 12–15 show the resulting magnitudes of heat flow and heat flux into the intermediate CO_2 store for each of the simulation series listed in Table 3. The heat flow was calculated as

$$Q_{\text{walls}} = 4 \cdot \int_{\partial\Omega} \mathbf{q} \cdot \mathbf{n} \, ds \tag{18}$$

where $\partial\Omega$ is the cavern wall surface, **q** is the heat flux vector through the surface and **n** is the outward unit normal vector to the surface. Multiplication by four was required since only one quadrant of the complete 3D geometry was modelled. The heat flux was then estimated by dividing the heat flow into the cavern by the total cavern wall surface area (Table 7). The cavern wall surface area was calculated by summing the individual areas of the triangles that made up the cavern walls in the finite element mesh.

Table 7. *Cavern wall surface areas for each CO_2 store design.*

Store design	Cavern wall surface area [m^2]
Single cavern of small cavern profile	11,424
Dual cavern of small cavern profile	12,106
Single cavern of large cavern profile	10,455
Dual cavern of large cavern profile	11,483

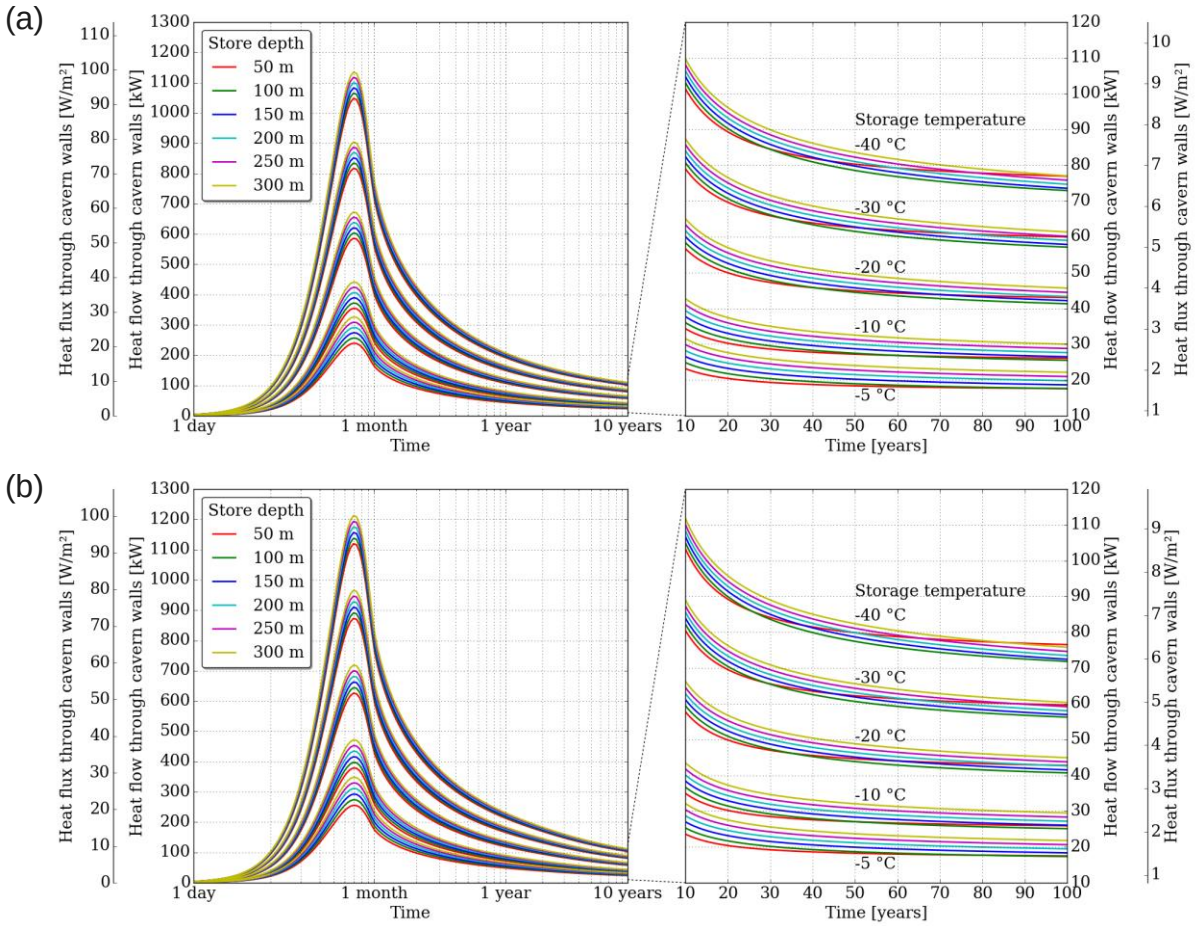

Figure 12. *Results of the simulation runs with no pre-cooling period for the (a) single and (b) dual cavern store designs of small cavern profile disregarding the effect of porosity (simulation series #1 and #2). The left panels show the first 10 years and the right panels the last 90 years of the simulation.*

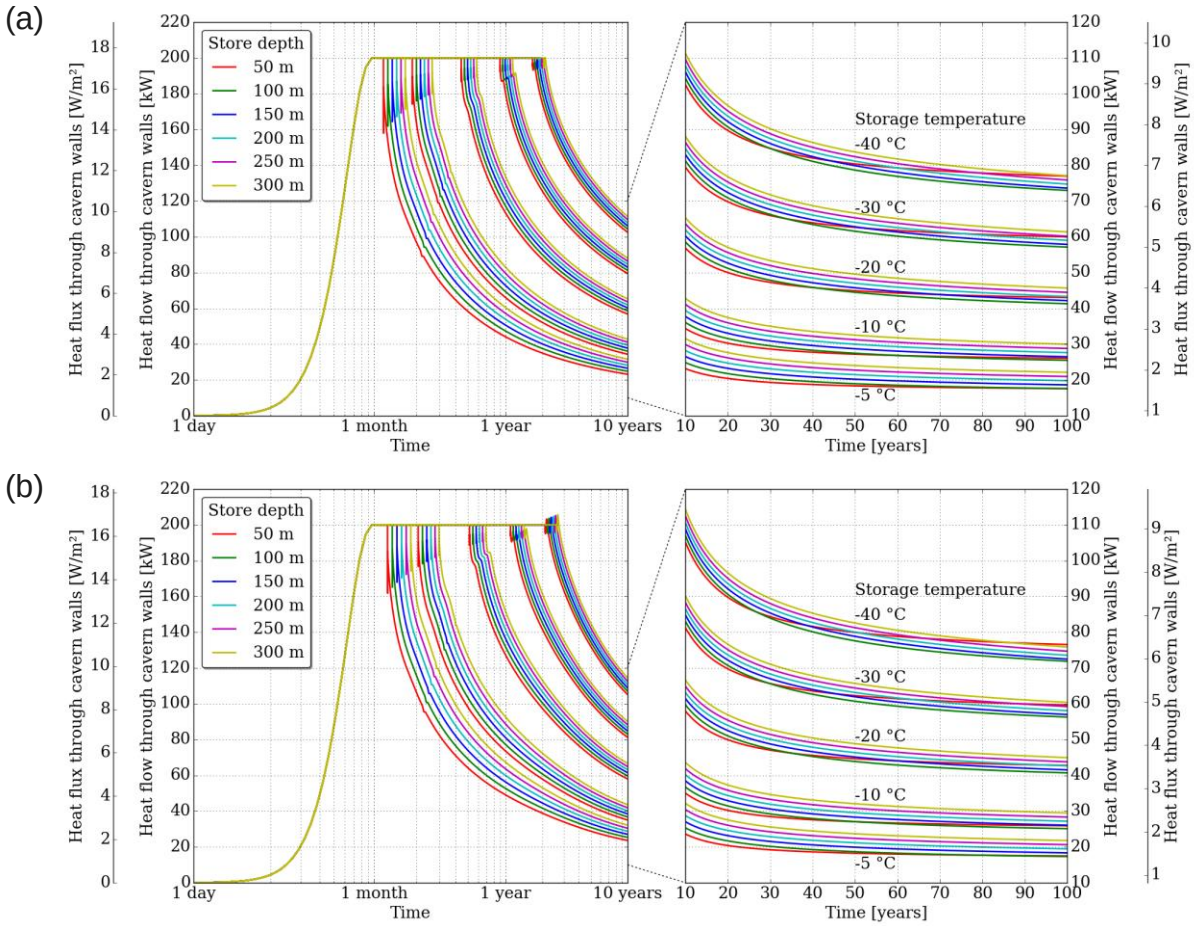

Figure 13. *Results of the simulation runs with a pre-cooling period for the (a) single and (b) dual cavern store designs of small cavern profile disregarding the effect of porosity (simulation series #3 and #4). The left panels show the first 10 years and the right panels the last 90 years of the simulation.*

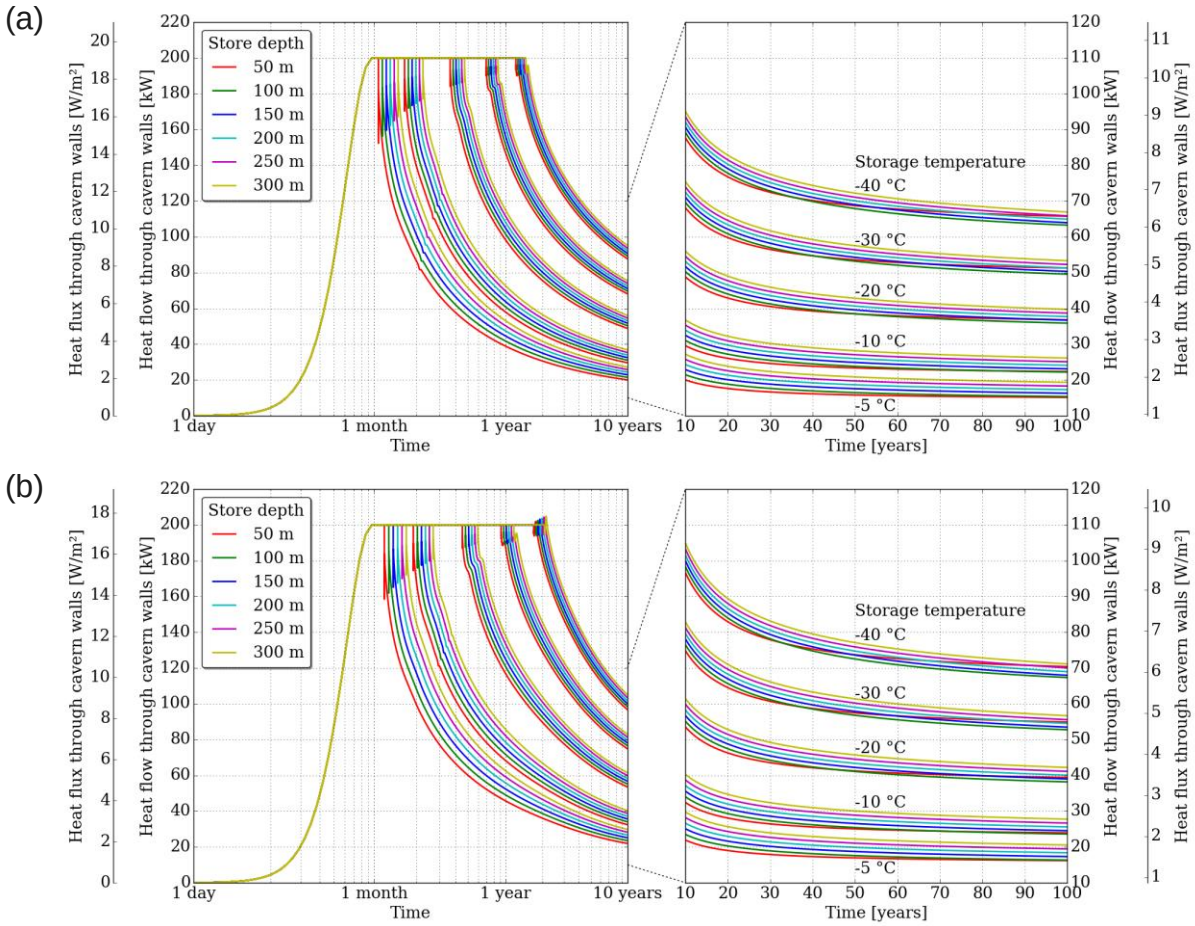

Figure 14. *Results of the simulation runs with a pre-cooling period for the (a) single and (b) dual cavern store designs of large cavern profile disregarding the effect of porosity (simulation series #5 and #6). The left panels show the first 10 years and the right panels the last 90 years of the simulation.*

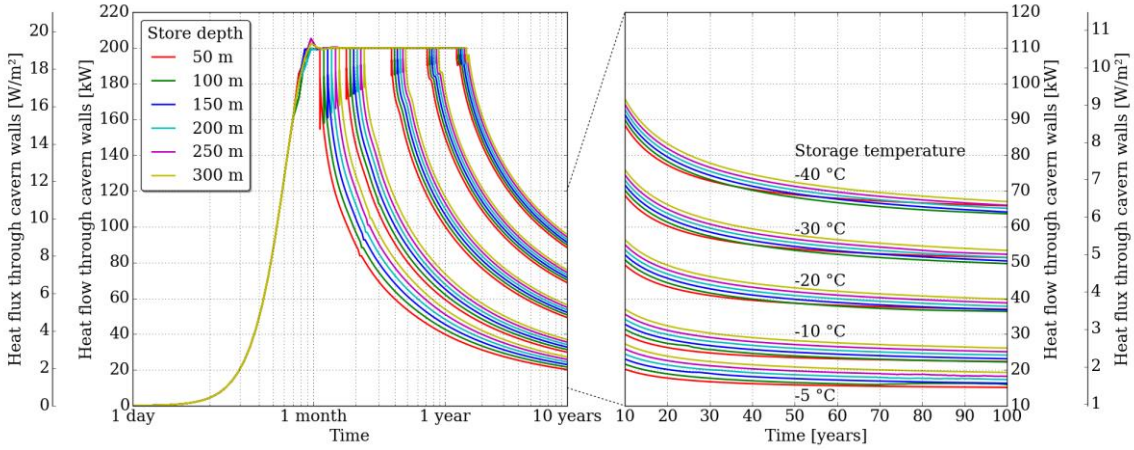

Figure 15. *Results of the simulation runs with a pre-cooling period for the single cavern store design of large cavern profile taking the effect of porosity into account (simulation series #7). The left panels show the first 10 years and the right panels the last 90 years of the simulation.*

5.2 Total energy consumption

Figures 16–19 illustrate the total energy consumption required to keep the store at the specified storage temperature during 100 years of simulation time as a function of store depth. The energy consumption was calculated as

$$E_{\text{total}} = \frac{10^{-9}}{3600} \cdot \int_{0}^{100 \cdot 365.2425 \cdot 3600} Q_{\text{walls}} \, dt \qquad (19)$$

whre E_{total} is the total energy consumption in gigawatt hours, Q_{walls} is the heat flow through the cavern walls in watts and t is the time in seconds.

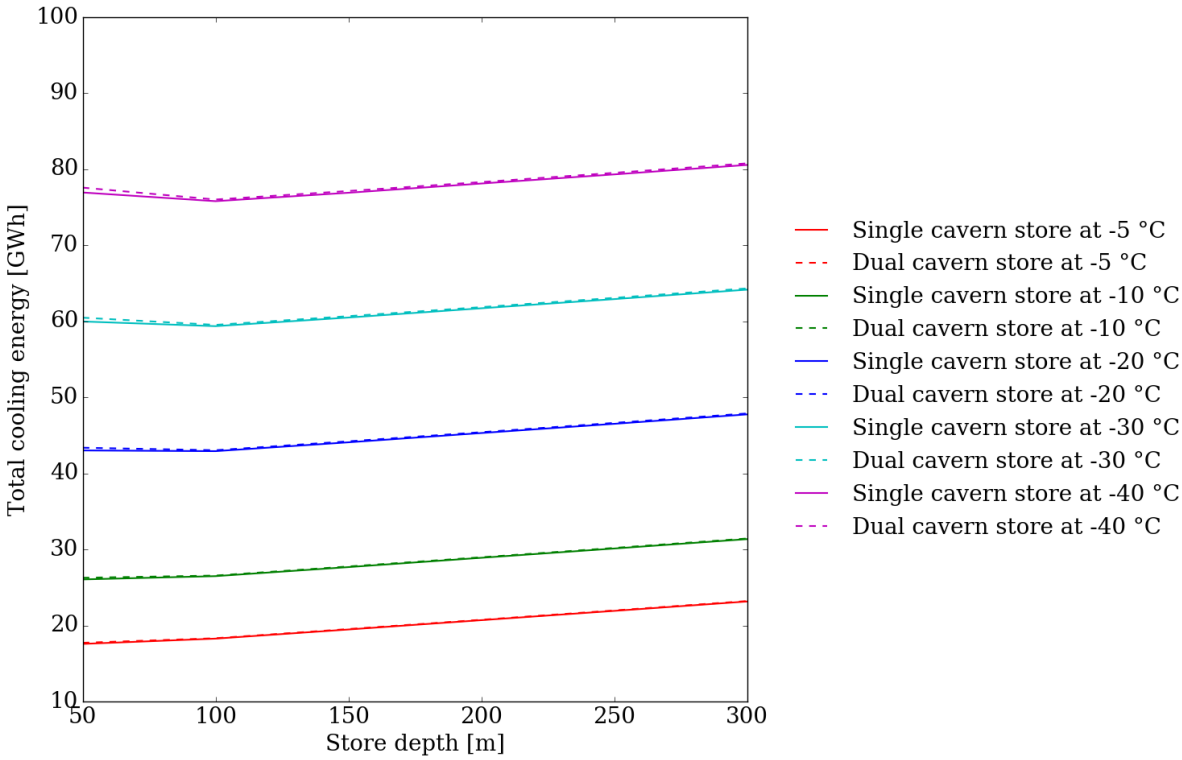

Figure 16. *Total energy consumption during 100 years of simulation time as a function of store depth for simulations of the single and dual cavern store designs of small profile size with no pre-cooling period disregarding the effect of porosity (simulation series #1 and #2).*

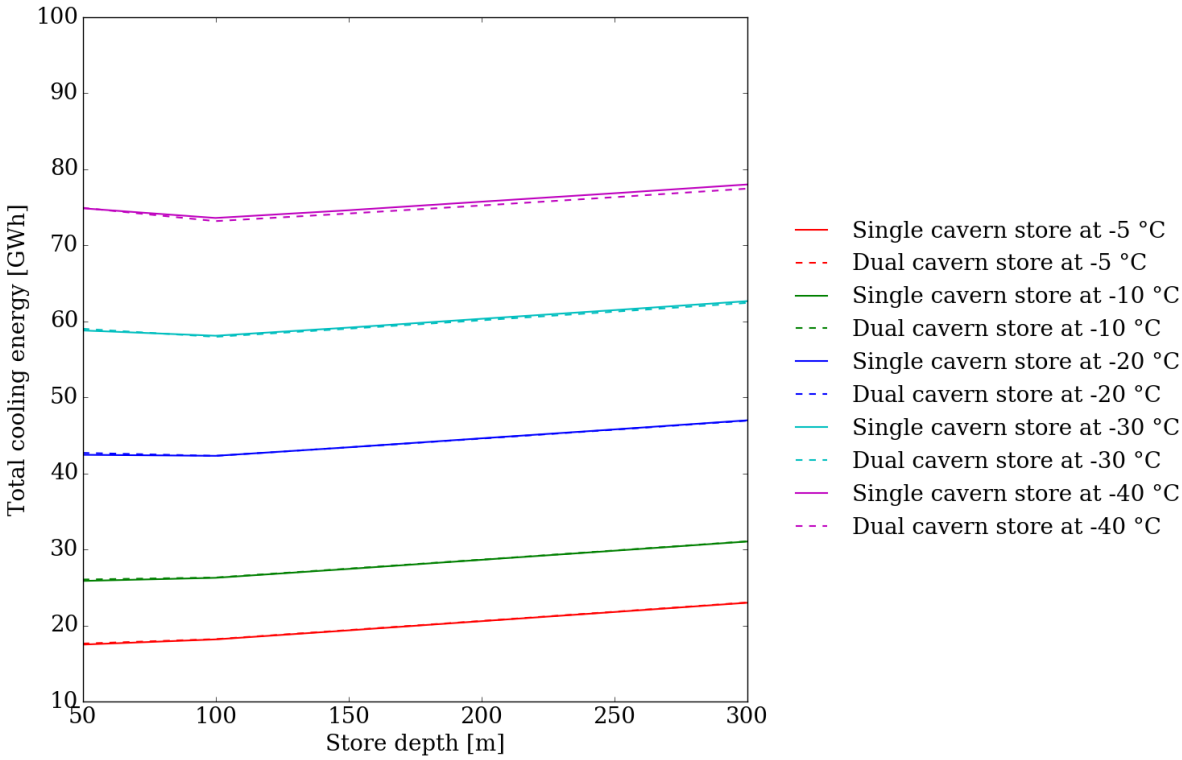

Figure 17. *Total energy consumption during 100 years of simulation time as a function of store depth for simulations of the single and dual cavern store designs of small profile size with a pre-cooling period disregarding the effect of porosity (simulation series #3 and #4).*

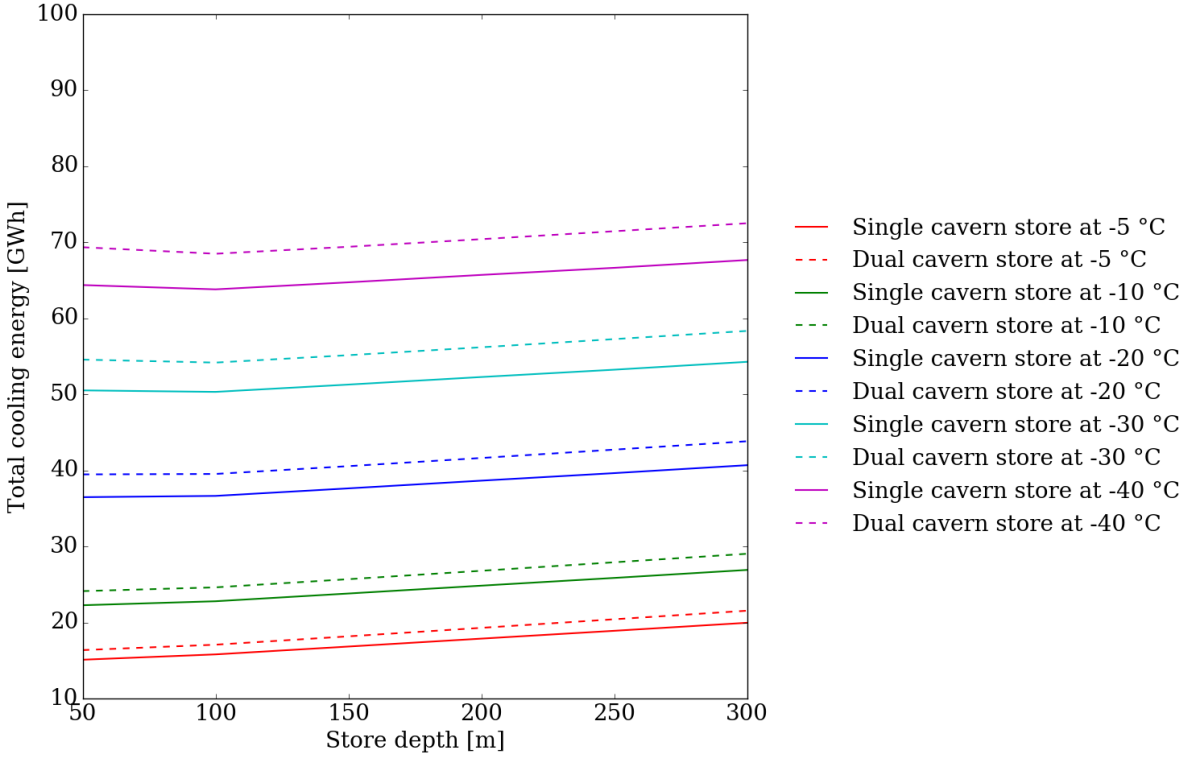

Figure 18. *Total energy consumption during 100 years of simulation time as a function of store depth for simulations of the single and dual cavern store designs of large profile size with a pre-cooling period disregarding the effect of porosity (simulation series #5 and #6).*

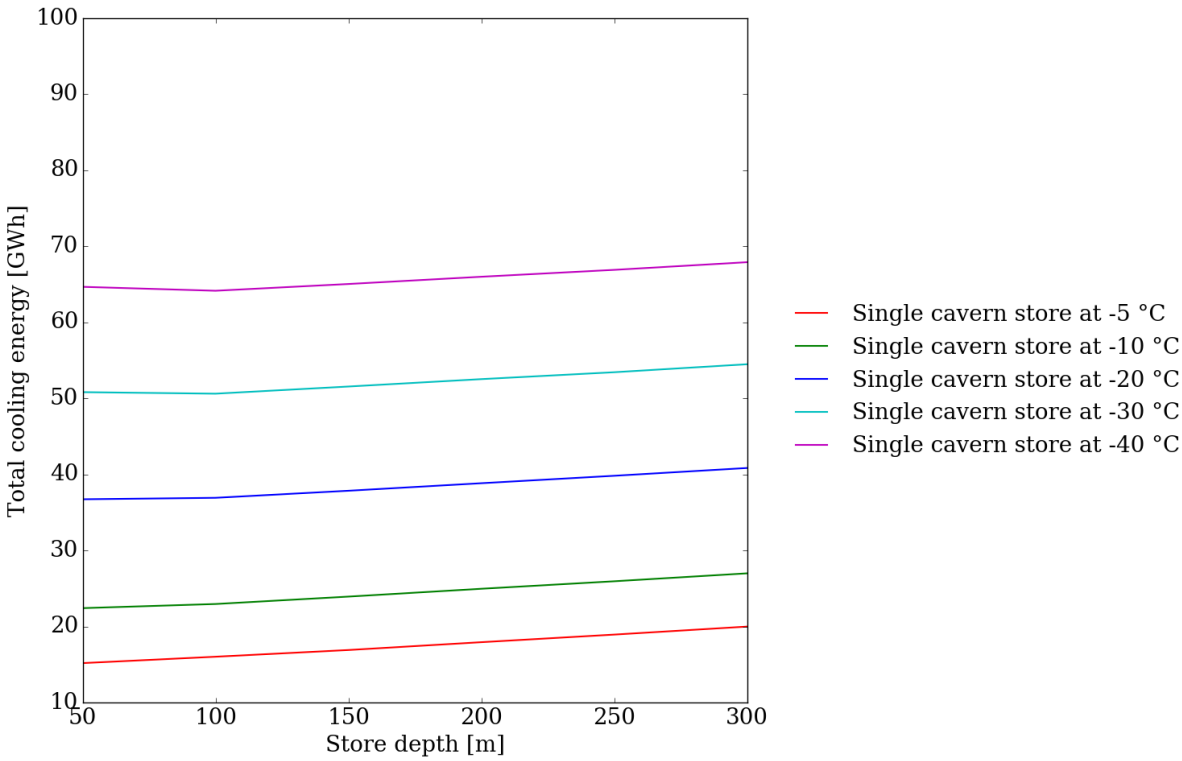

Figure 19. *Total energy consumption during 100 years of simulation time as a function of store depth for simulations of the single cavern store designs of large profile size with a pre-cooling period taking the effect of porosity into account (simulation series #7).*

5.3 Frozen zone thickness

Figures 20–23 illustrate the thickness of the frozen zone after 1 and 100 years of simulated time. The frozen zone thickness was calculated in the following way. First, the points approximating the zero-centigrade isotherm were calculated on the *xz* symmetry plane. Then, the distances between all the combinations of these points and the points defining the cavern profile on the xz symmetry plane were calculated. Finally, the frozen zone thickness was taken to be the smallest of the calculated distances.

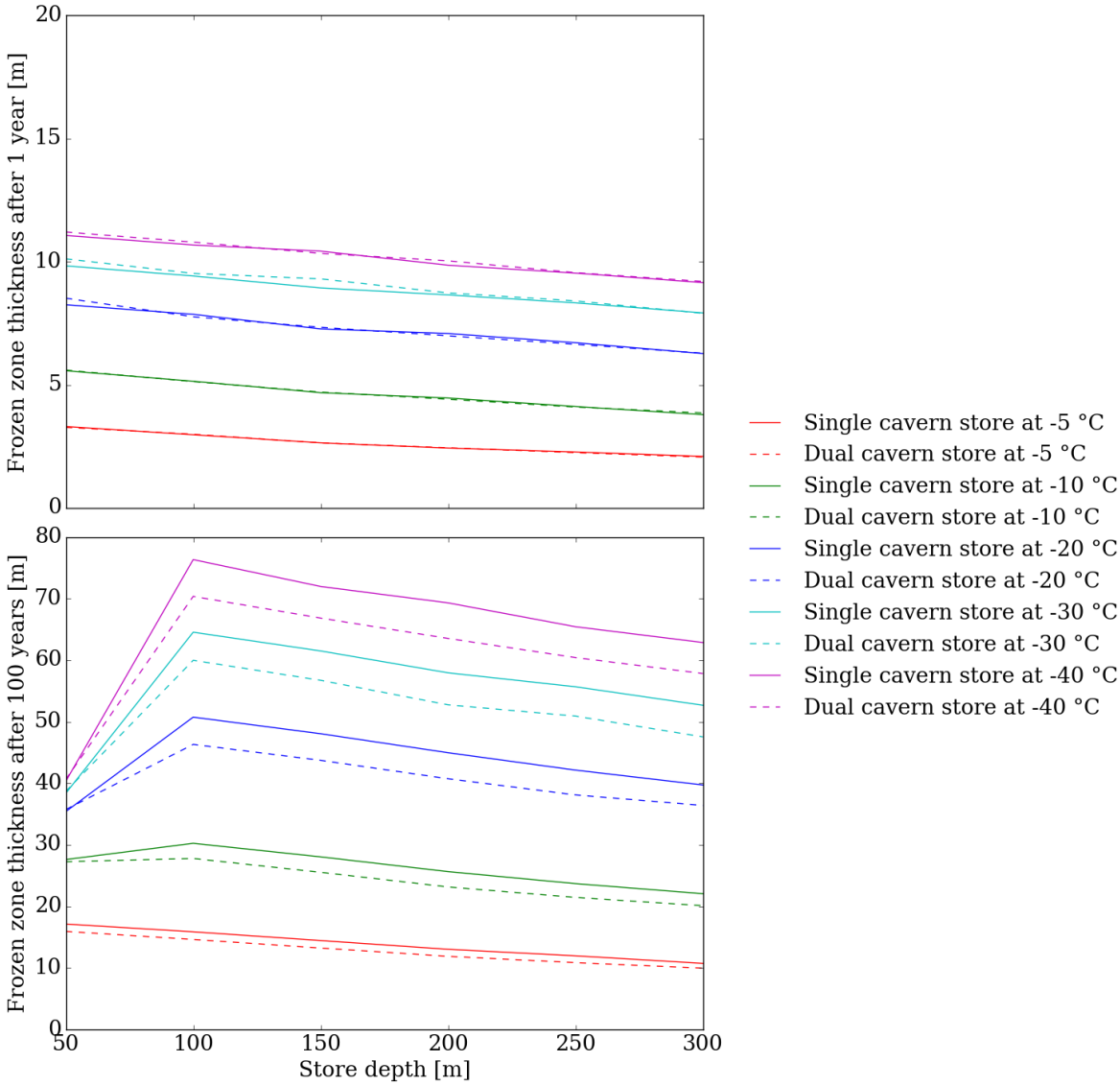

Figure 20. *Frozen zone thickness after 1 year (upper panel) and 100 years (lower panel) for simulations of single and dual cavern stores of small cavern profile size with no pre-cooling period and disregarding the effect of porosity (simulation series #1 and #2).*

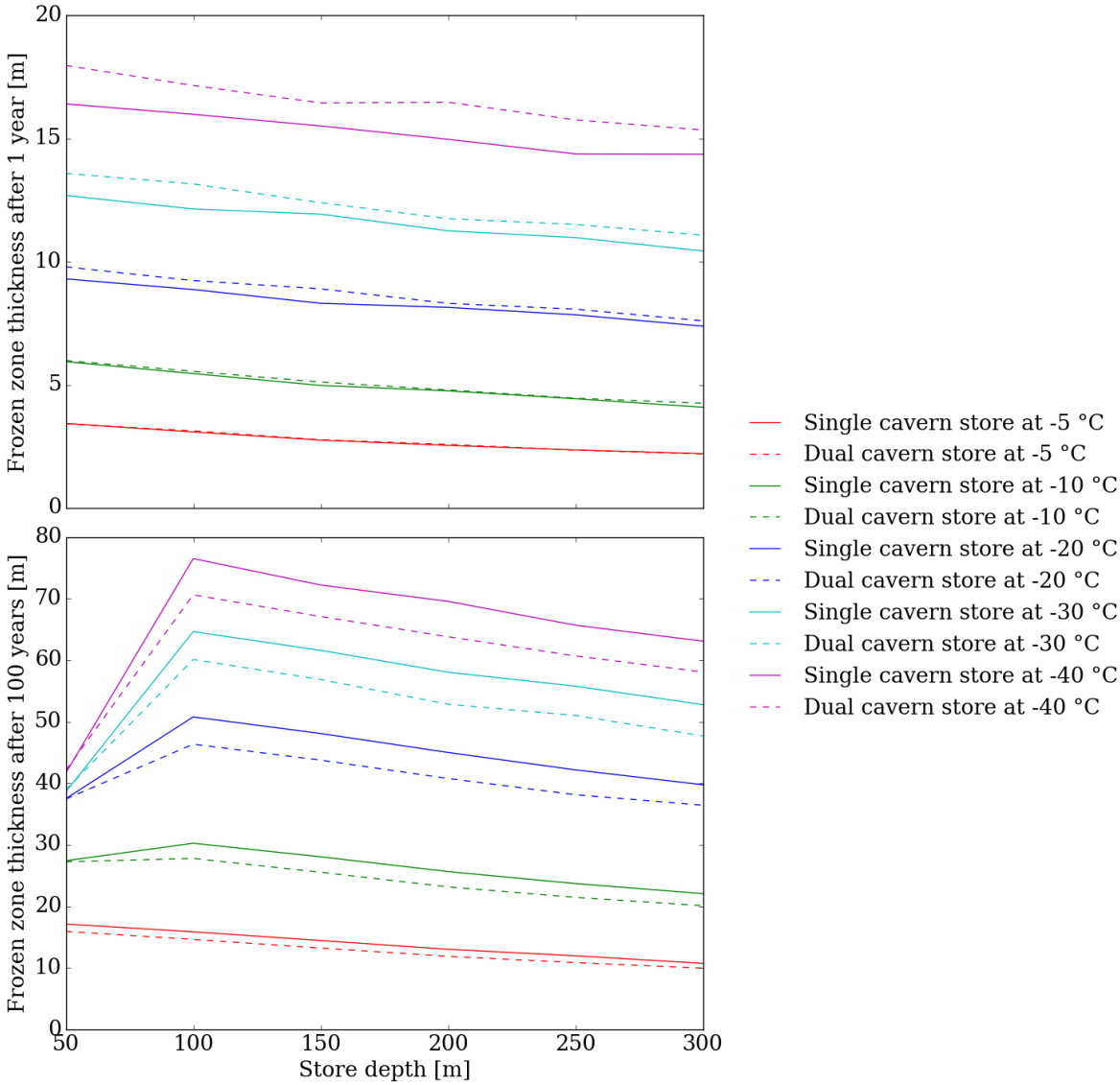

Figure 21. *Frozen zone thickness after 1 year (upper panel) and 100 years (lower panel) for simulations of single and dual cavern stores of small cavern profile size with a pre-cooling period and disregarding the effect of porosity (simulation series #3 and #4).*

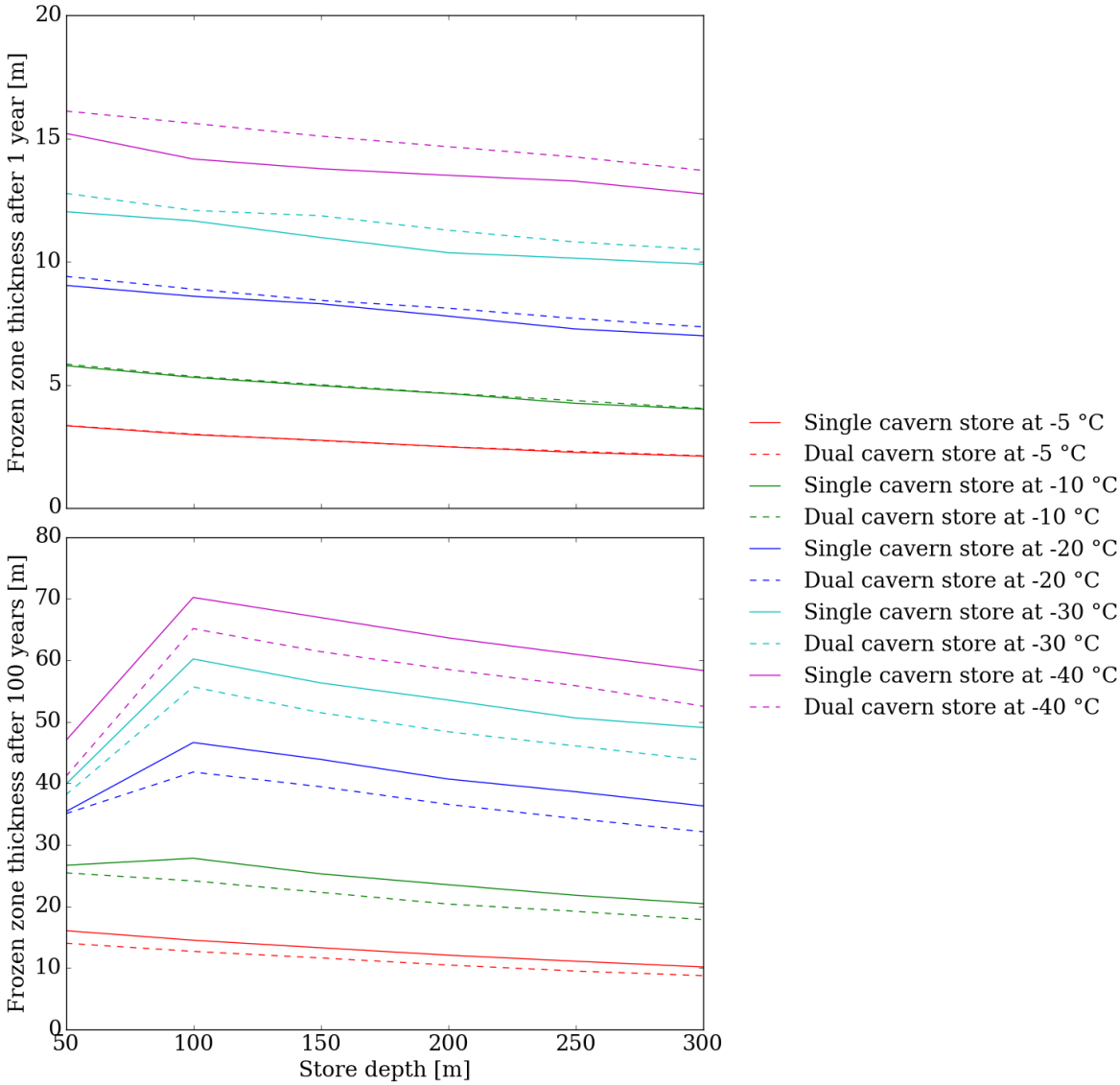

Figure 22. *Frozen zone thickness after 1 year (upper panel) and 100 years (lower panel) for simulations of single and dual cavern stores of large cavern profile size with a pre-cooling period and disregarding the effect of porosity (simulation series # and #6).*

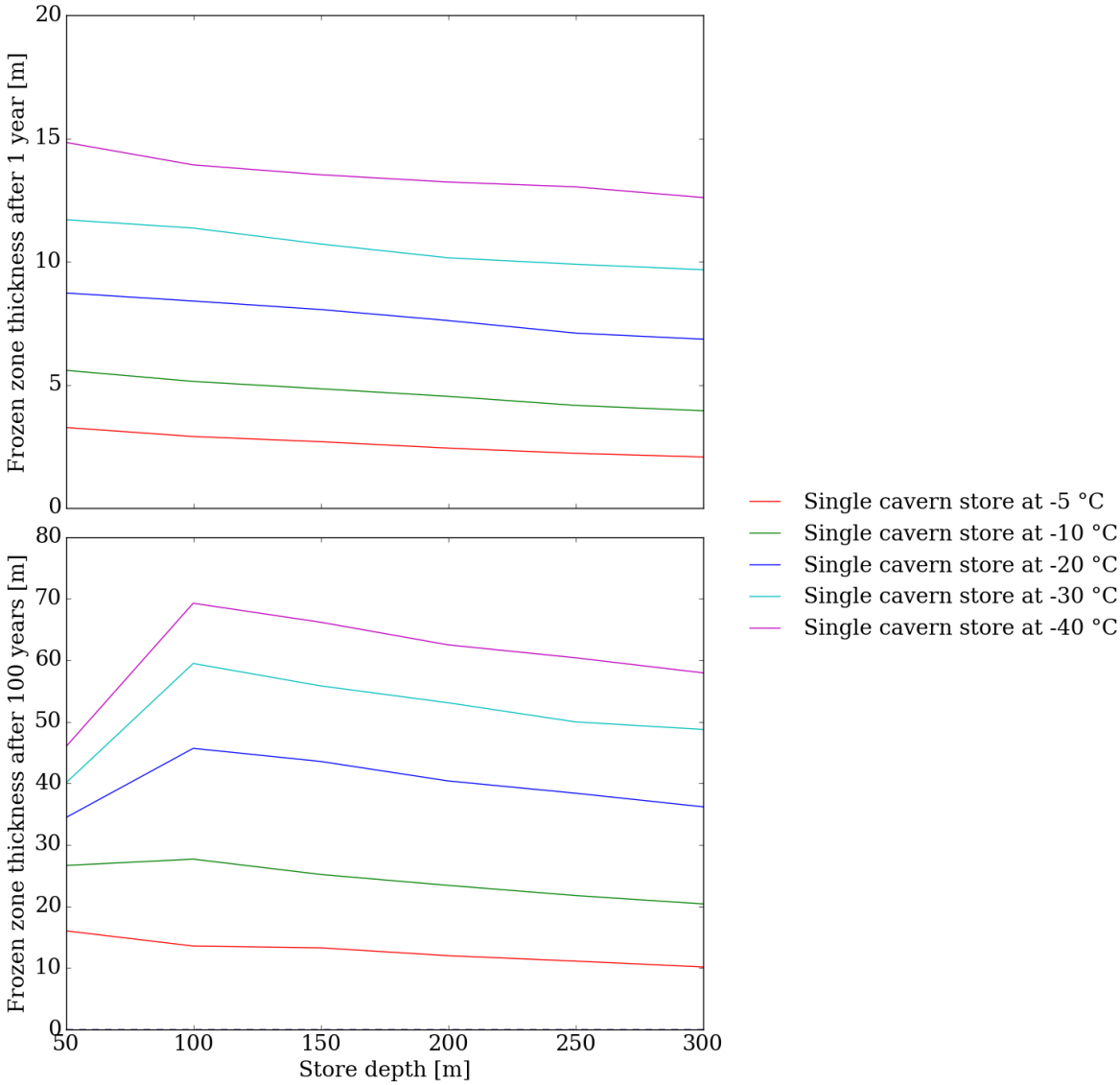

Figure 23. *Frozen zone thickness after 1 year (upper panel) and 100 years (lower panel) for simulations of single cavern stores of large cavern profile size with a pre-cooling period and taking the effect of porosity into account (simulation series #7).*

6 Summary and conclusions

The simulations containing no pre-cooling period indicate a heat-flow peak of even 1.0–1.2 MW into the store (Fig. 12). Approximately after one year of storage, the magnitudes of the heat flows drop below 200 kW (Fig. 12). That is, in storage scenarios with no pre-cooling period, a considerable amount of energy is required to keep the CO_2 in its liquid form. This heat-flow peak lasts only for a short period considering the entire life-cycle of the store. Thus, a more reasonable choice would be to cut the heat-flow peak by pre-cooling the bedrock in the vicinity of the store using a constant cooling capacity which is closer to the long-term energy demand (Figs. 13–15).

The CO_2 storage temperature has a significantly higher influence on the total energy demand than the store depth (Figs. 16–19). The total energy demand grows 14–17 GWh per 10 K drop in the storage temperature while it grows only 1–2 GWh per 50-meter increase in the store depth. The increase in energy demand as the store depth grows is related to the geothermal gradient (the increase in ground temperatures as a function of depth).

Similarly, the growth of the frozen zone is more significantly influenced by the CO_2 storage temperature than the store depth (Figs. 20–23). In general, the storage temperature has 5–10 times larger influence on the thickness of the frozen zone than the store depth. However, if the store is located at the depth of 50 meters, the heat flux through the ground surface significantly inhibits the growth of the frozen zone especially if the storage temperature is low (Figs. 20–23).

The differences in the heat flows (and, consequently, in the energy consumption and growth of the frozen zone) between the simulations ran using the single and dual cavern store models are due to differences in the surface area of the cavern walls. The models with smaller cavern surface area are more favorable as they have a smaller area through which heat is transferred to the store. This can, especially, be seen by comparing the single cavern model runs shown in Figs. 13 and 14, Figs. 17 and 18, and Figs. 21 and 22.

The influence of porosity in the heat flows to the stores is insignificant. This can be seen by comparing the single cavern model runs shown in Figs. 14 and 15, Figs. 18 and 19, and Figs. 22 and 23.

Bedrock that is poor on calcite, such as the granitic and gneissic bedrock of Finland, is the most suitable host for intermediate CO_2 stores. The optimal store geometry is obviously one that minimizes the surface area of the caverns. The optimal store depth needs to be chosen considering the following issues. A thick frozen zone around the intermediate CO_2 store is favorable as it helps to seal the CO_2 inside the store and prevent CO_2 from mixing with groundwater. The lower the storage temperature, the thicker the frozen zone becomes. However, lower storage temperatures induce larger heat flows into the store requiring more energy as more BOG needs to be re-liquefied. But, if the frozen zone is not thick enough, the BOG may escape to the atmosphere through fractures if the gas pressure exceeds the prevailing hydrostatic pressure at the store depth (see Tables 1 and 2). That is, the higher the CO_2 storage temperature, the deeper the store would need to be located.

During the life-cycle of an intermediate CO_2 store, the degree to which the store is filled will vary as CO_2 gets shipped away to the final storage site and the store again gets re-filled as new CO_2 arrives. However, as boil-off constantly occurs, the store will be filled with a mixture of liquid and gaseous CO_2. Thus, the temperature inside the store is likely to remain close to the CO_2 storage temperature even if the store is not completely filled with liquid CO_2.

We propose the following general emplacement strategy for intermediate CO_2 stores excavated in hard rock. The store should be located at or below the depth of 100 meters. This is because shallow stores will be strongly influenced by solar and atmospheric heating through the ground surface which will inhibit the growth of the frozen zone around the store. Furthermore, the prevailing hydrostatic pressure at shallow depths is low and, thus, requires a low CO_2 storage temperature in order to safely seal the CO_2 inside the store. The carbon dioxide storage temperature should be −20 °C or lower so that the CO_2 vapor pressure would not be too high, and that the frozen zone would grow thick enough to seal the CO_2 safely inside the store. Based on the prevailing hydrostatic pressure and CO_2 vapor pressure we propose the following.

- The CO_2 storage temperature of −40 °C is promoted for stores located at the depths between 100 and 150 meters (highest demand of energy in order to keep CO_2 liquid).
- The CO_2 storage temperature of −30 °C is promoted for stores located at the depths between 150 and 200 meters.
- The CO_2 storage temperature of −20 °C is promoted for stores located below the depth of 200 meters (lowest demand of energy in order to keep CO_2 liquid).

A more comprehensive emplacement strategy would require also rock mechanical studies and the modeling of the stresses induced by the freezing of water. These would provide information about the integrity of the frozen zone, the risk of tensile fracturing and the ice thawing of rocks at different depths and CO_2 storage temperatures. Rock mechanical aspects strongly depend on the existing geological structures and the current stress field. Therefore, geological and rock mechanical site investigations would be required at the possible intermediate CO_2 storage sites.

7 References

Ritola, J., Kujanpää, L., Lindberg, A., and Nordkbäck, N., 2014. CLEEN - CCS Task 4.21. CO_2 – Terminals and Intermediate storage. CLEEN Ltd., Final Report 2013, 42 p.

Leung, Dennis Y.C., Caramanna, G., and Maroto-Valer, M. Mercedes, 2014. An overview of current status of carbon dioxide capture and storage technologies. Renewable and Sustainable Energy Reviews, 39, 426–443.

Fang, Y., Baojun, B., Dazhen, T., Dunn-Norman, S., and Wronkiewicz, D., 2010. Characteristics of CO_2 sequestration in saline aquifers. Petroleum Science, 7, 83–92.

Myer, L., 2011. Global status of geologic CO_2 storage technology development. United States Carbon Sequestration Council, Report March 7, 2011, 58 p.

Ahn, J., Headly, M., Wahlen, M., Brook, E.J., Mayewski, P. A., and Taylor, K.C., 2008. CO_2 diffusion in polar ice: observations from naturally formed CO_2 spikes in the Siple Dome (Antarctica) ice core. Journal of Glaciology 54, 685–695.

Bateman, K., Rochelle, C.A., Purser, G., Kemp, S.J., and Wagner, D., 2013. Geochemical interactions between CO_2 and minerals within the Utsira caprock: A 5-year experimental study. Energy Procedia, 37, 5307–5314.

Johansson, S., 1985. Engineering geological experience from Finland from unlined excavated oil storage caverns in a Precambrian rock mass in the Porvoo area, Southern Finland. Doctoral dissertation, University of Turku. Neste Oy, Finland. 77 p.

Deardorff, J.W., 1978. Efficient Prediction of Ground Surface Temperature and Moisture with Inclusion of a Layer of Vegetation. Journal of Geophysical Research 83, 1889–1903.

Nocedal, J., Wright, S.J., 2006. Numerical Optimization. Springer, New York, NY. 2nd edition.

Gilgen, H., and Ohmura, A., 1999. The Global Energy Balance Archive (GEBA). Bulletin of the American Meteorological Society 80, 831–850.

Seemann, S.W., Borbas, E.E., Knuteson, R.O., Stephenson, G.R., Huang, H.-L., 2007. Development of a Global Infrared Land Surface Emissivity Database for Application to Clear Sky Sounding Retrievals from Multi-spectral Satellite Radiance Measurements. Journal of Applied Meteorology and Climatology 47, 108–123.